Use of a stereo-topometric measurement system for the characterization of rock joint roughness in-situ and in the laboratory

B.S.A. Tatone & G. Grasselli
Lassonde Institute, University of Toronto, Toronto, Ontario, Canada

ABSTRACT: The surface roughness of unfilled rock discontinuities has a major influence on the deformational and hydraulic behaviour of discontinuous rock masses. Although it is widely recognized that surface roughness is comprised of large-scale (waviness) and small-scale (unevenness) components, most investigations of surface roughness have been restricted to small fracture surfaces (< $1m^2$). Hence, the influences of the large-scale components of roughness are often neglected. Furthermore, these investigations typically focus on analyzing roughness in terms of two-dimensional profiles rather than the complete three-dimensional geometry, which can lead to potentially biased estimates of roughness. This contribution demonstrates the use of a new optical digital measurement system, based on the principle of triangulation, to digitize a large-scale natural rock discontinuity surface at both outcrop-scale (~6m x 2m) and lab-scale (~100mm x 100mm). Subsequently, the digitized surfaces are systematically analyzed using the three-dimensional roughness methodology proposed by Grasselli to investigate the dependency of roughness on sample window size and measurement resolution.

1 INTRODUCTION

It has long been recognized that the roughness of rock discontinuities, when clean and unfilled, have a significant impact on both the hydraulic and shear strength characteristics of discontinuous rock masses. In response, several attempts have been made to develop shear strength criteria that account for the effect of surface roughness; the most well known criteria being those of Barton (1973), Ladanyi & Archambault (1970) and Patton (1966).

It is widely recognized that the mechanical behaviour of rough rock joints varies as a function of scale, albeit the extent is arguable (Bandis et al. 1981, Hencher et al. 1993). This scale-dependant behaviour is partly attributed to the variation of asperity strength and partly to the variation in surface geometry (roughness) with scale (Barton & Choubey 1977).

Although it is generally agreed that discontinuity roughness is comprised of a large-scale waviness component and a small-scale unevenness component (ISRM 1978), most investigations of surface roughness and scale effects have generally focused on joint samples less than $1m^2$. Hence, large-scale roughness components are rarely measured and accounted for when considering the mechanical behaviour of field-scale discontinuities (Fardin et al. 2001).

In addition to inadequately sized fracture surfaces, roughness investigations have suffered from the conventional approach of attempting to characterize three-dimensional (3D) geometry via two-diemensional (2D) linear profiles. This approach, although capable of characterizing pseudo-3D geometry when several profiles in various directions are considered, can lead to incomplete and biased representations of the surface (Rasouli & Harrison 2004, Riss & Gentier 1990). Moreover, it is very time consuming when used to characterize large surfaces (Grasselli et al. 2002).

In recent years, several optical techniques including laser scanners and photogrammetric systems have emerged as an attractive alternative for measuring discontinuity surfaces for roughness determination. With such tools, it is possible to rapidly obtain highly accurate, high resolution 3D point clouds defining both small-scale surfaces in the laboratory and large-scale surfaces in-situ. To date, despite these technological advances, few studies have investigated the roughness of large-scale fractures in-situ (Fardin et al. 2004, Feng et al. 2003, Haneberg 2007, Maerz & Franklin 1990).

The objective of the current study is two-fold. Firstly, it aims at investigating the dependency of roughness on sample size by digitizing a large-scale natural fracture surface in-situ and evaluating the roughness of sample windows of varying size. Secondly, it considers the effect of measurement resolution on roughness by digitizing a series of small-scale fractures specimens at different resolutions in the laboratory and evaluating the roughness. In both cases, digitization is performed using a stereo-topometric scanner (ATOS II by GOM mbH) and the 3D roughness is characterized according to the method proposed by Grasselli (Grasselli 2006, Grasselli & Egger 2003, Grasselli et al. 2002). This study represents the first time that both the ATOS II and Grasselli's roughness method have been employed to characterize a large-scale natural fracture surface.

2 MEASUREMENT EQUIPMENT AND METHODOLOGY

2.1 *3D digitization equipment: the ATOS II by GOM mbH*

For this study, a 3D stereo-topometric measurement system, the Advanced Topometric Sensor (ATOS) II manufactured by GOM mbH, was adopted to digitize a large-scale fracture surface in-situ and three small-scale samples in the laboratory. The ATOS II and its predecessors were initially developed for quality control and reverse engineering in the automotive industry (GOM 2008). However, the system has now been used for a wide range of measuring applications including the characterization of lab-scale rock fracture surfaces (Grasselli 2006, Hong et al. 2006, Nasseri et al. 2009).

The ATOS II system consists of a measurement head containing a central projector unit and two CCD cameras, and a high-performance Linux-based PC to pilot the system. The system is flexible in that it can be used in the laboratory with a boom-type stand and industrial PC or in the field with a laptop and tripod. Figure 1 illustrates the laboratory and field set-up of the ATOS II for the current study. It is noted that due to the lack of availability of a suitable laptop, the industrial PC was transported in a vehicle and powered via a portable generator to operate the system in the field for the current study (Fig. 1b).

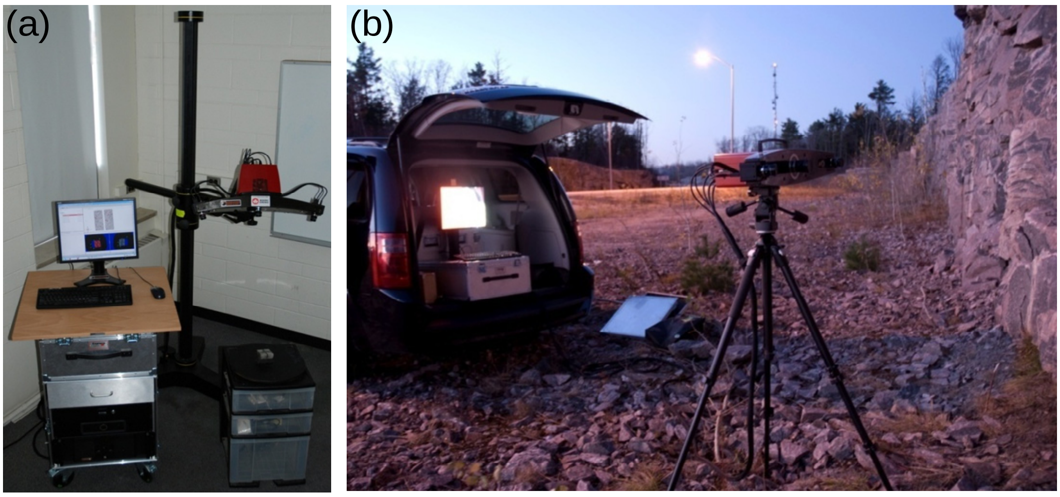

Figure 1. The 3D stereo-topometric measurement system utilized for this study, the Advanced Topometric Sensor (ATOS) II manufactured by GOM mbH: (a) lab configuration and; (b) field configuration.

The ATOS II measures 3D coordinates by projecting various structured white-light fringe patterns onto the surface. Images of these patterns, which become distorted due to the relief of the surface, are captured automatically by the two CCD cameras. From the left and right images, the software computes precise 3D coordinates for each pixel based on the principle of triangulation. Since the resolution of the CCD cameras are 1392 x 1040 pixels, the system used for the current study is capable of measuring up to roughly 1.4 million points in one measurement (GOM 2008). Depending on the selected camera shutter speeds, the completion of one measurement typically takes between 1 and 10 seconds.

The average spacing (resolution) of the measurement points and total measurement volume that can be digitized in one measurement are varied by changing the lenses of the CCD cameras and projector and varying the offset between the cameras. The current study utilized four different lens and projector configurations. The average point spacing, measuring volume, and measuring distance (distance from the sensor to the surface) corresponding to each of these configurations is summarized in Table 1.

Table 1. Summary of measuring volume, point spacing, and measuring distance of the four ATOS II configurations employed in the current study.

ATOS Configuration	Measuring volume (*l* x *w* x *h*) (mm^3)	Average point spacing (mm)	Measuring distance (mm)
1	1400 x 1120 x 952	1.0	1400
2	700 x 560 x 476	0.5	1030
3	350 x 280 x 238	0.25	1030
4	55 x 44 x 37.5	0.04	280

Since the system can only calculate 3D coordinates for the pixels which are visible in both the left and right images, complete digitization of a surface typically requires several individual measurements from different angles or positions. To properly position each of these measurements into a common global coordinate system requires the use of reference points (adhesive circular markers), which are applied directly to the surface to be digitized. Based on the first measurement, the system establishes an arbitrary global coordinate system and identifies any reference points in the field of view. For all subsequent measurements, the system automatically identifies new and previously measured reference points and uses the previously measured points to automatically transform the current measurement into the global coordinate system. Following the first measurement, at least three previously measured reference points must be visible in each successive measurement to properly transform the measurement into the global coordinate system (GOM 2008).

Following digitization, the 3D measurement data can be exported from the ATOS system as a point cloud or polygonized surface in a variety of file formats. For the current study, the digitized fracture surfaces were reconstructed using the default triangulation algorithm (Delaunay triangulation with no smoothing) and exported in *STL* format for subsequent roughness analysis. This approach discretizes the surface into contiguous triangles with vertices defined by neighbouring points of the point cloud and orientations defined by the normal vector of each triangle (Fig. 2).

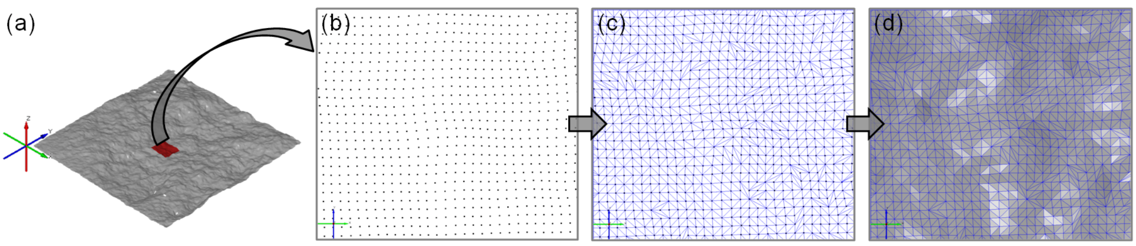

Figure 2. Triangulation of the measured point cloud: (a) 3D view of triangulated point cloud; (b) zoomed-in view of original point cloud; (c) connection of points to their natural neighbours to form triangular elements; and (d) the rendered triangular mesh to be exported in *STL* format for roughness analysis.

2.2 *In-situ fracture digitization*

To study the scale-dependency of discontinuity roughness, a large fracture surface exposed in a relatively new road-cut (~5 years) was digitized in-situ with the ATOS II. Although various ATOS systems have previously been used to investigate rock fracture roughness, this study marks the first time the system has been used to digitize a fracture surface in-situ. As shown in Figure 3, the rock-cut is located roughly 200km north of Toronto, Ontario, Canada along the north-bound off ramp of Exit 189 of Highway 400 (45°05’37”N, 79°46’54”W). The rock-cut extends nearly 200m through a medium-grained granite gneiss rock mass and reaches a maximum height of approximately 7m. The cut face is oriented sub-parallel to a persistent sub-vertical fracture set that strikes roughly NNE-SSW. As a result, the face contains several large exposures of planar to undulating natural fracture surfaces with slight alteration (Fig. 3c).

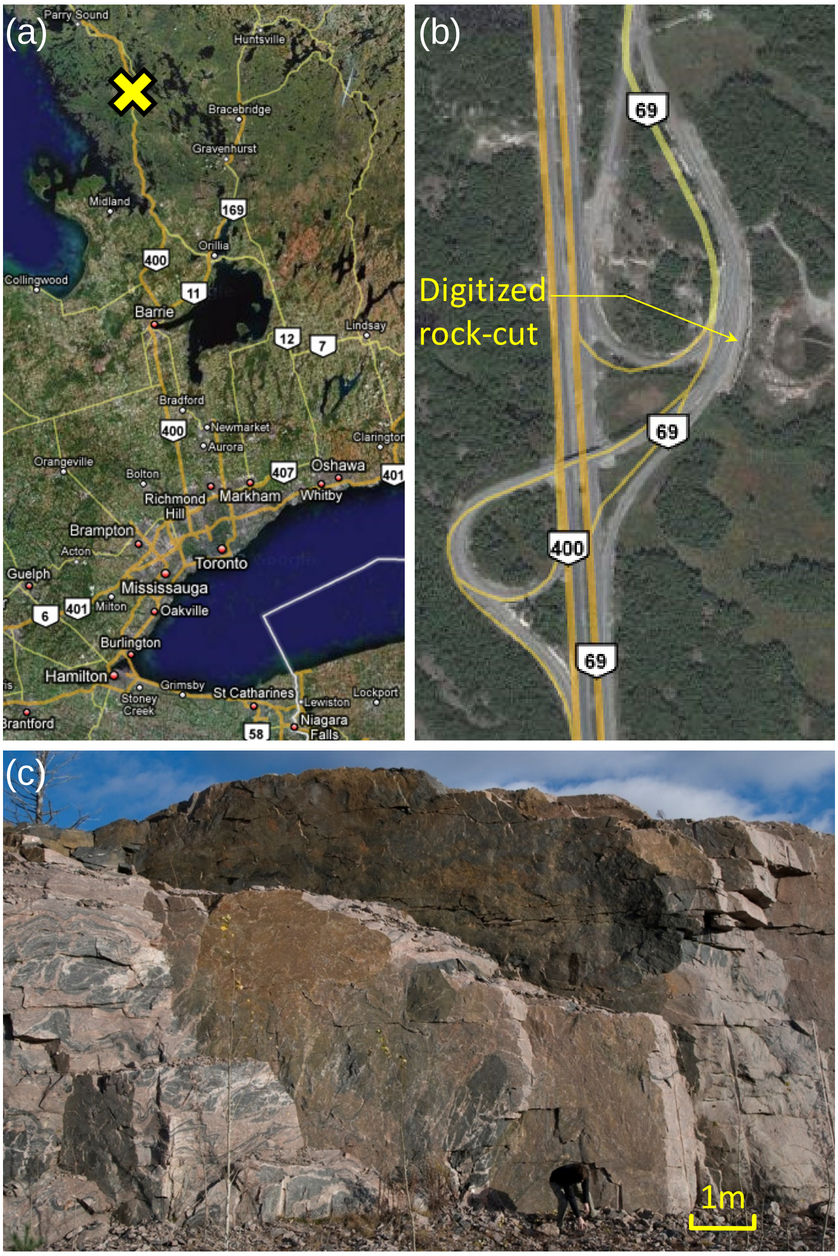

Figure 3. Location and description of large-scale fracture surface digitized in-situ: (a) regional map marking the location of the rock cut; (b) aerial photo showing digitized rock-cut; and (c) example of the large natural fracture surfaces exposed in the rock-cut.

For the current study, a total area measuring approximately 6m wide and 2m high was digitized using the first configuration listed in Table 1. As shown in Figure 4, the digitized area consisted of two large fracture surfaces separated by a 0.3m step. These two surfaces were digitized individually and subsequently merged together into one large 3D model (Fig. 4b). Starting from the centre of each surface and working radially outwards, as demonstrated in Figure 4a, 10 measurements were needed to digitize each surface. Transformation of each measurement into a common global coordinate system was achieved using a 0.6m x 0.6m grid of 12mm diameter reference points affixed to the fracture surface with a small amount of epoxy. The 3D model of the entire digitized area, as shown in Figure 4b, contains approximately 8.2 million points and 16.3 million triangles. The computed mesh deviation of this model was 0.181mm. As this value quantifies the average deviation between redundant data (i.e. overlapping measurements), it serves as an estimate of the intensity of the average measurement noise in the 3D data (GOM, 2008).

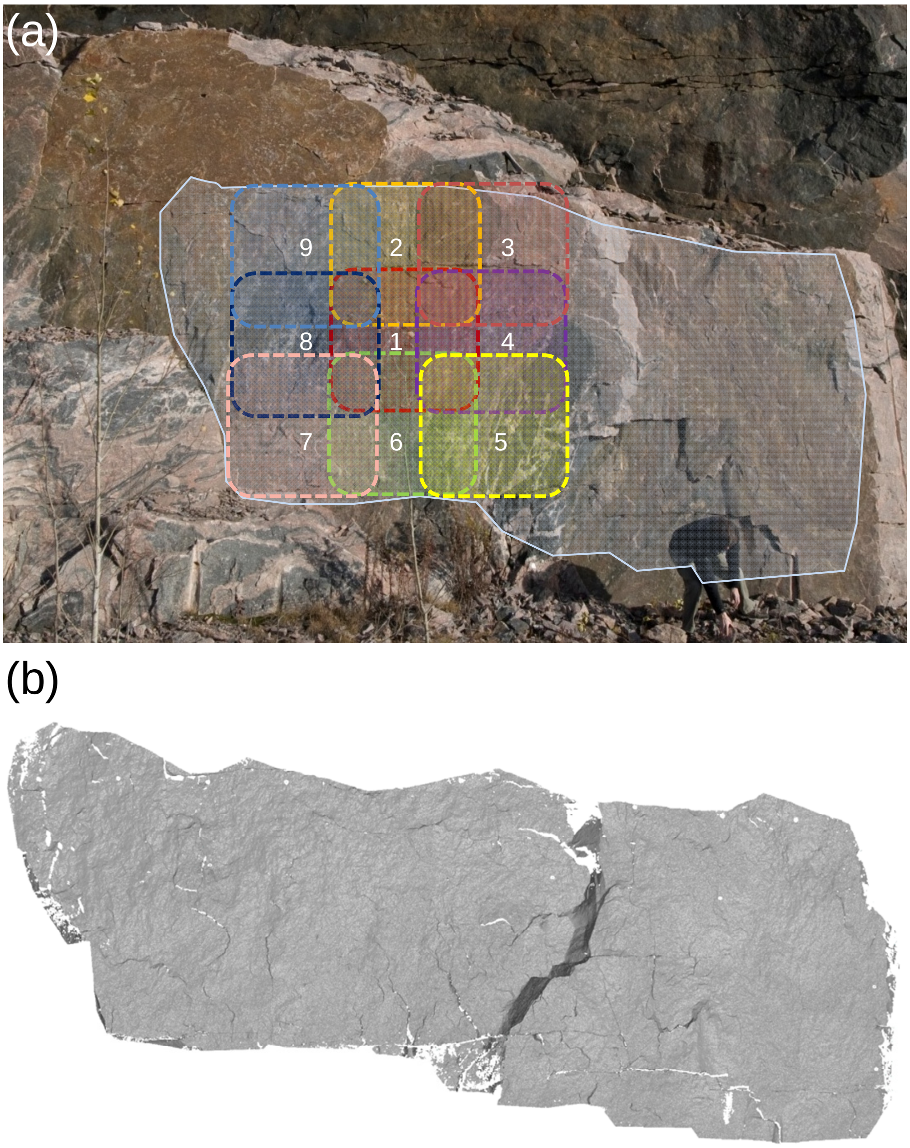

Figure 4. Total area digitized with the ATOS II: (a) demonstration of the digitization sequence starting in the centre of the left fracture surface and working radially outwards according to the number sequence indicated; and (b) the complete 3D model of the fracture surface defined by 8.2 million measurement points with an average spacing of 1mm.

Remembering that the system uses fringe projection to calculate 3D coordinates, the projected patterns had to be clearly visible when photographed by the CCD cameras. As bright ambient lighting can create significant problems in this regard, it was decided that the measurement of the fracture be carried out in the evening (Fig. 5). The total time required for two people to perform the data acquisition in the field was nearly 1.5 hours; 0.5hrs of equipment unloading and setup, 0.5 hours to place all the reference points on the surface, and 0.5 hours to take the 20 measurements. Considering that this field work represented the first time the authors used the ATOS II in the field, it is anticipated that digitization of a similar sized area in the future could be accomplished in less than one hour.

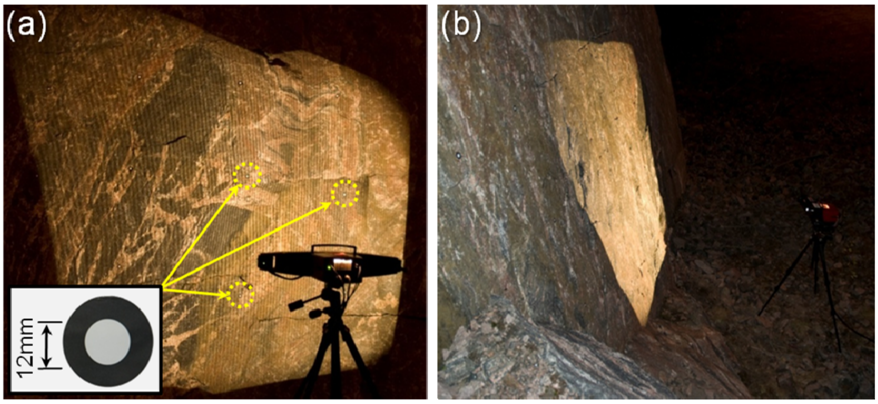

Figure 5. In-situ digitization process: (a) projection of fringes onto the rock face, 12mm reference points affixed to the face; and (b) alternate view of ATOS II measuring the large-scale fracture surface in-situ.

2.3 *Digitization of small-scale samples of the large-scale fracture surface*

To study the impact of measurement resolution on roughness estimates, three small-scale samples (Fig. 6a, b) of the large-scale fracture surface were collected during the in-situ digitization process and transported to the University of Toronto. In the laboratory, these samples were digitized using each configuration listed in Table 1. Considering the measuring volume of the first three configurations relative to the size of the samples, complete digitization required only one or two measurements. Thus, only four to seven 5mm reference points were needed around the perimeter of each sample to permit transformation. Conversely, the fourth configuration (0.04mm point spacing) had a significantly smaller measuring volume; hence, digitization of each sample required several measurements. Similar to the field procedure, the surface of each sample was digitized by working radially outwards from the centre, transforming each measurement into a common coordinate system via 0.4mm reference points placed on the surface (Fig. 6c). Digitization with the fourth configuration also required the surfaces to be lightly dusted with talc powder, as shown in Figure 6c, to reduce overexposure caused by shiny mineral grains.

Following digitization, the 3D models corresponding to each measurement resolution were transformed into a common coordinate system via common reference points. Afterwards, square sampling windows, as outlined in Figure 6b, were exported for roughness analysis. The total number of measurement points and range of computed mesh deviations for each of these windows is summarized in Table 2.

Table 2. Summary of the total number of measurement points and corresponding mesh deviations obtained with each ATOS configuration upon digitization of the sampling windows illustrated in Figure 6b.

Configuration	Measurement points			Mesh deviation
	Sample 1	Sample 2	Sample 3	(mm)
1	5586	10,079	10,270	0.05
2	19,289	34,551	34,823	0.020-0.025
3	154,565	279,586	279,711	0.010-0.013
4	2,622,181	4,809,868	4,897,906	0.004-0.006

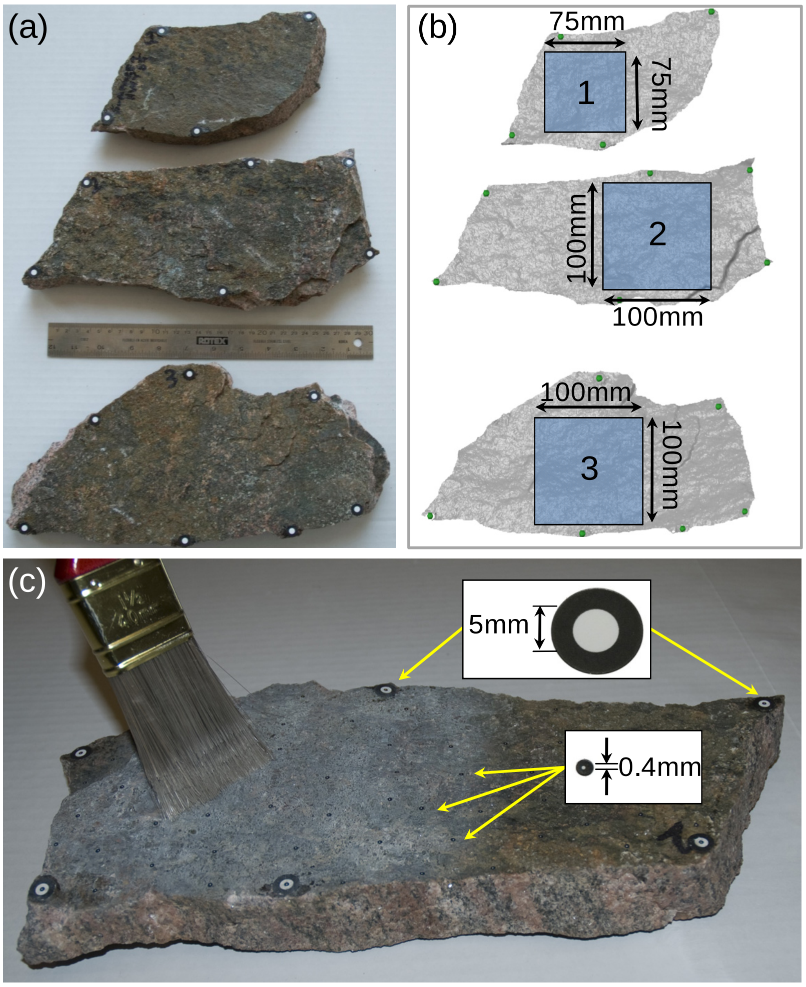

Figure 6. (a) Three small-scale fracture samples digitized at varying resolution; (b) Example of digitized surface of samples along with the square sampling windows considered for roughness analysis; (c) Example of the 5mm and 0.4mm reference points and talc powder brushed on to surfaces to dull shiny minerals.

3 ROUGHNESS QUANTIFICATION METHODOLOGY

To arrive at an objective description of roughness requires further analysis of the 3D surface measurements. In this paper, 3D roughness is characterized using the angular threshold concept developed by Grasselli (2006) and Grasselli et al. (2002, 2002b). This method, which was initially developed as a means of identifying potential contact areas during direct shear testing of artificial tensile rock fractures, characterizes roughness based on the distribution of the apparent inclination of the individual triangular elements of an *STL* file defining a surface.

After establishing a least squares best-fit plane through the entire surface and specifying an analysis direction of interest, the orientation of each triangular element can be uniquely identified by its dip, θ, and azimuth, α. The dip is defined as the maximum angle between the best-fit plane and the individual triangles, while the azimuth is defined as the angle measured clockwise between the selected analysis direction and the projection of the true dip vector, ***d***, onto the best-fit plane (Fig. 7).

Given the dip and azimuth, it is possible to define the apparent inclination of each triangle with respect to the specified analysis direction. This apparent inclination is termed the apparent dip angle, θ^*, and is obtained by projecting the true dip vector, ***d***, onto a vertical plane oriented along the analysis direction, ***t*** (Fig. 7). Mathematically, the apparent dip is related to the true dip according to (1):

$$\tan\theta^* = -\tan\theta \cdot \cos\alpha \,. \tag{1}$$

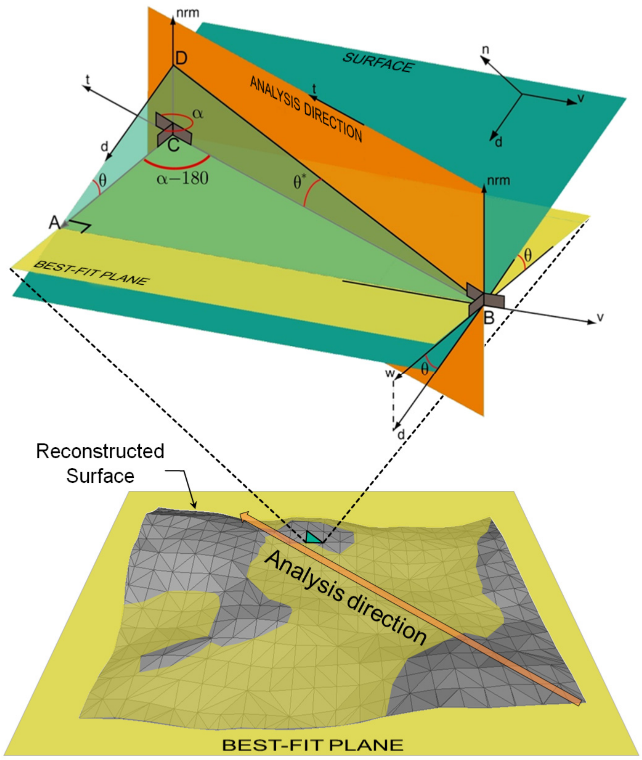

Figure 7. Schematic diagram illustrating the geometric definition of azimuth, dip and apparent dip in relation to the selected analysis direction (Grasselli 2006, Grasselli et al. 2002).

Based on the apparent dip angle of each triangular element, it is possible to distinguish the fraction of the surface area (normalized to the total surface area), $A_{\theta*}$, that is more steeply inclined than a given threshold value of θ^*. By considering several angular thresholds between 0° to 90° (the upper and lower bound values), it is possible to characterize the cumulative distribution of the normalized area, $A_{\theta*}$, as a function of θ^*. The relationship between $A_{\theta*}$ and the threshold apparent dip angle can be expressed by (2):

$$A_{\theta*} = A_0 \left(\frac{\theta^*_{\max} - \theta^*}{\theta^*_{\max}} \right)^C , \tag{2}$$

where A_0 is the normalized area of the fracture corresponding to a threshold angle of 0°; θ^*_{max} is the maximum apparent dip angle of the surface in the chosen analysis direction; and C is an empirical fitting parameter, calculated via a non-linear least-squares regression, that characterizes the shape of the distribution (Grasselli et al. 2002). The resulting area under the best-fit curve defined by Equation (2) is found to characterize the relative roughness of the surface. The expression for the area under the curve is given by the definite integral of Equation (2):

$$A_0 \int_0^{\theta^*_{\max}} \left(\frac{\theta^*_{\max} - \theta^*}{\theta^*_{\max}} \right)^C d\theta^* = A_0 \left(\frac{\theta^*_{\max}}{C+1} \right). \tag{3}$$

Since A_0 is found to be roughly 0.5 for all surfaces, the unique variable in this expression for the area under the curve is defined by $\theta^*_{max}/(C+1)$. Therefore, this value is adopted as the measure of roughness in the selected analysis direction. To fully characterize the surface and visualize anisotropy in roughness, the parameters A_0, C and θ^*_{max} are calculated in several possible directions (from 0° to 360° in 5° increments) and the resulting values of $\theta^*_{max}/(C+1)$ are plotted in a polar diagram (Grasselli et al. 2002).

4 INVESTIGATION OF ROUGHNESS SCALE-DEPENDENCE

4.1 *Effect of sampling window size*

To investigate the effect of scale on the 3D surface roughness of the large-scale fracture surface described previously, the digitized surface was systematically analyzed according to the roughness quantification method described in the preceding section of this paper (Section 3). From the complete digital surface model (Fig. 4b), several square and rectangular sampling windows were analyzed to examine the sensitivity of the 3D roughness parameters to the size of the sampling window. Figure 8a and b illustrate the location of the various square and rectangular sampling windows considered, respectively. Recalling that the selected roughness quantification approach requires a best-fit plane through the surface as a reference plane, a unique best fit plane was determined for each sample window. In all cases, the best fit plane was set as the *xy*-plane (z = 0) with the positive y-axis oriented in the up-dip direction along the line of maximum dip and the positive x-axis oriented in the strike direction (according to the right-hand rule).

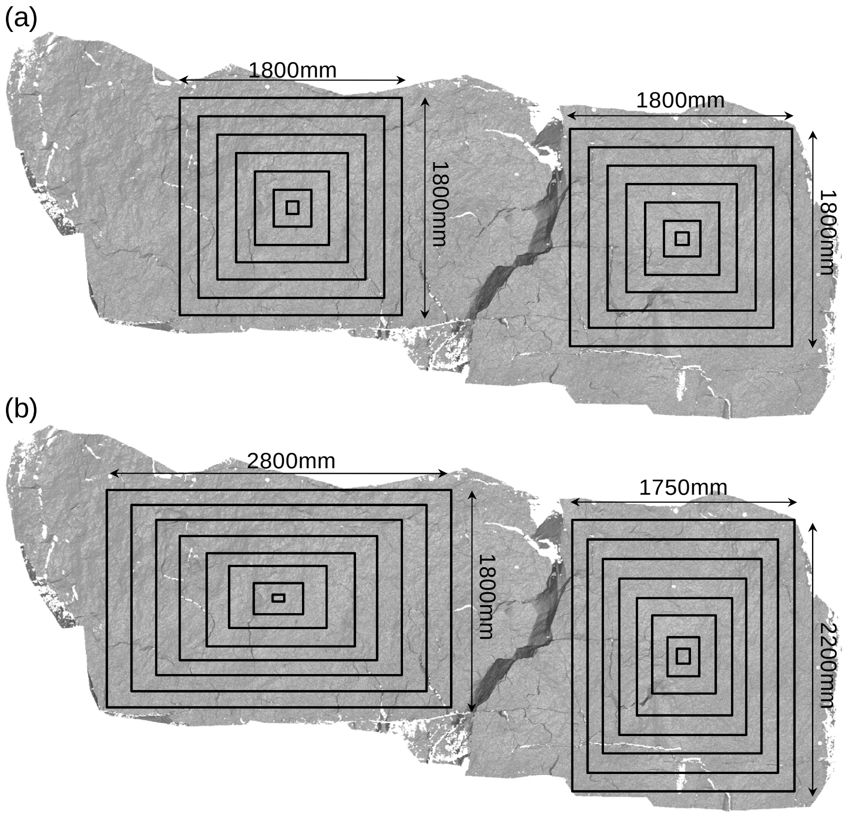

Figure 8. (a) Locations of square sampling windows (100mm x 100mm to 1800mm x 1800mm); (b) Location of rectangular sampling windows (left: 100 x 64mm to 2800mm x 1800mm and right: 100mm x126mm to 1750mm x 2200mm)

The resulting 3D roughness calculated for each sampling window is displayed on the four polar plots in Figure 9. Comparison of the plots for the left (Fig. 9a, c) and right (Fig. 9b, d) surfaces shows that the variation in roughness over the range of window sizes considered is fairly consistent and the influence of window shape (i.e. square vs. rectangular) on the resulting plots is minimal. Looking closely at the polar plots, it is evident that, generally, the 3D roughness increases with expanding window size (positive scale effect). The plot of average roughness as a function of sampling window size (Fig. 10a) further illustrates this trend. A percent difference of nearly 37% is observed between the roughness values obtained for the smallest window (100 x 64 mm^2) and largest window (1750 x 2200 mm^2). Additionally, the plot of average roughness indicates that scatter in roughness values decreases with increasing window size and that the roughness appears to be approaching a constant value of roughly 8 units for windows greater than $3x10^6$ mm^2. Therefore, considering the fracture surface examined in this study, uncertain and potentially misleading roughness estimates needed for rock engineering design purposes can be avoided by evaluating a sample area greater than or equal to this threshold size. The upper bound sample size can be limited to the block size of the rock mass similar to the approach of Bandis et al. (1981).

Considering the elliptical shape of all data series plotted in Figure 9, all sampling windows display a fairly consistent anisotropy, in which lower roughness values are observed along the line of maximum dip (90° - 270°) and higher values in the perpendicular direction (0° - 180°). Defining anisotropy as the ratio of maximum to minimum roughness, the anisotropy as a function of sample size is plotted in Figure 10b. Similar to roughness, the scatter in anisotropy decreases with increasing sample window size; however, over the entire range of window sizes it remains close to 1.2 suggesting it is relatively scale-insensitive.

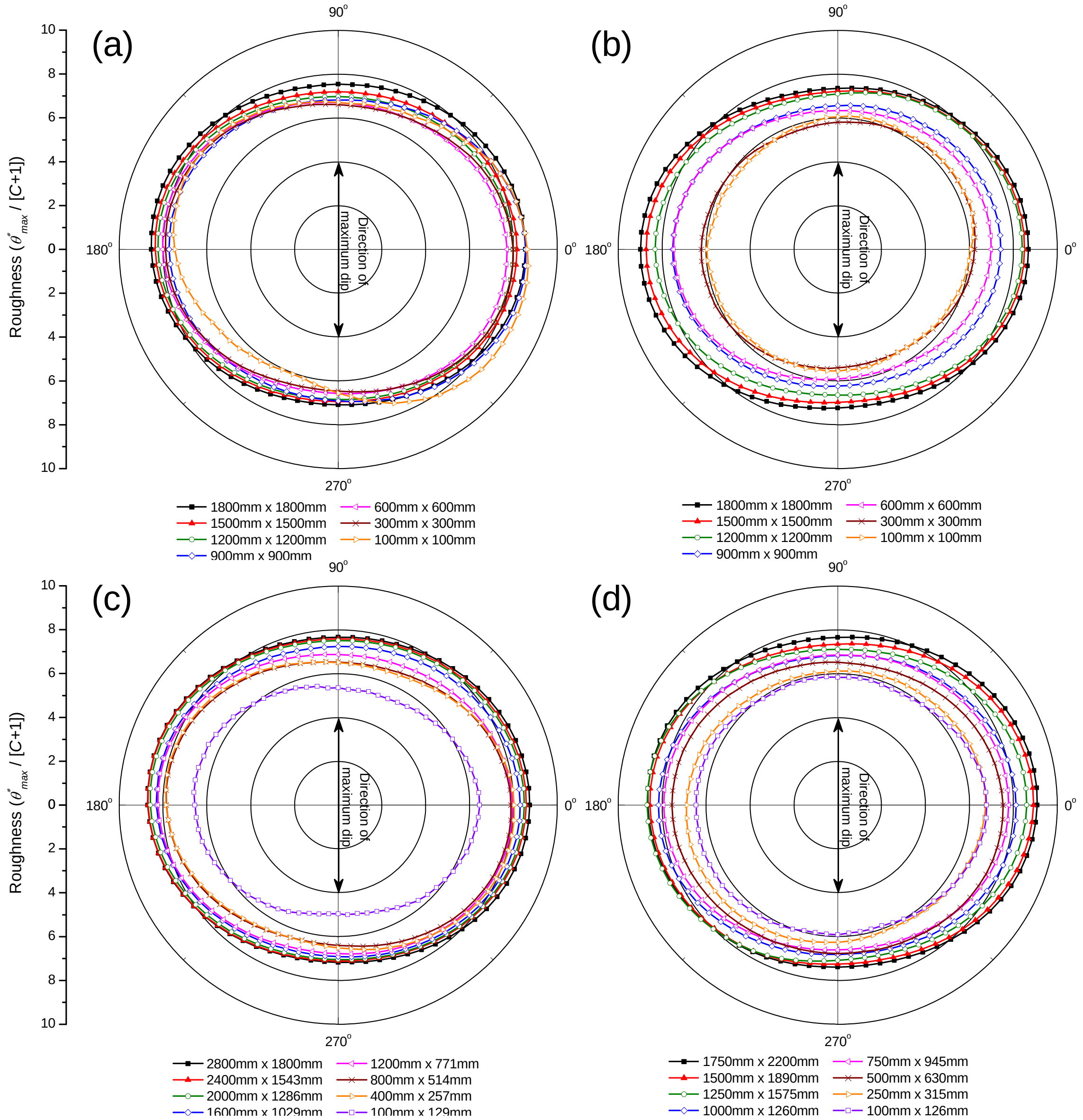

Figure 9. Polar plots of the roughness value, $\theta^*_{max}/(C+1)$, for the sampling windows of various size defined in Figure 8. (a) and (b) represent the left and right square sampling windows, respectively; while (c) and (d) represent the left and right rectangular sampling windows, respectively.

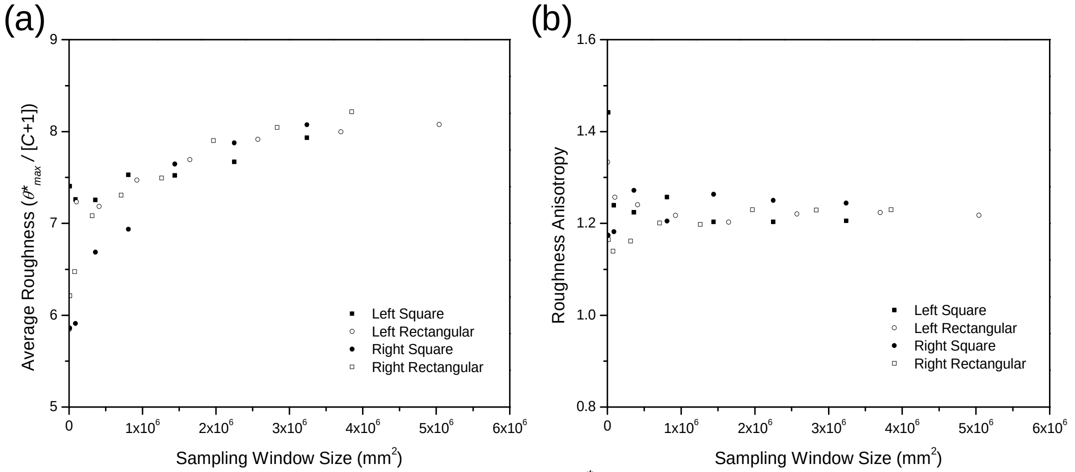

Figure 10. (a) Plot of the average roughness value, $\theta^*_{max}/(C+1)$, as a function of sampling window size. (b) Plot of roughness anisotropy as a function of sampling window size.

4.2 *Effect of measuring resolution*

To examine the role of measurement resolution on surface roughness, each small-scale sample was digitized with four different measurement resolutions (Table 1) and analyzed according to the 3D roughness method previously described. Considering the square sampling windows defined in Figure 6b, comparison of the 3D surface models obtained at different resolutions qualitatively illustrate that increasing the point spacing acts to smooth the fracture surface (e.g. Fig. 11). Results of the 3D roughness analysis support this qualitative observation. Figure 12 displays the polar plots of the 3D roughness for the three samples at each resolution. All three samples display a similar decrease in roughness with increased point spacing. Considering the average values of roughness as a function of point spacing, as plotted in Figure 13a, a sizable percent difference of 79% to 85% is observed when the average spacing of measurement points is varied between 0.04mm and 1mm.

The elliptical shape of the polar plots indicates there is anisotropy in roughness. Plotting the anisotropy as a function of measurement point spacing illustrates that, although there is increased scatter with increased resolution, it remains close to 1.2 which is similar to the value observed for the in-situ surface (Fig. 12b). However, unlike the polar plots obtained from the in-situ fracture surface, these plots indicate there is less roughness in the 0° - 180° direction versus the 90° - 270° direction. This discrepancy is explained by the orientation of the samples relative to the direction of maximum dip. Although the exact line of maximum dip was not recorded on the surface of the small-scale fracture samples in the field, the horizontal direction with respect to Figure 6 roughly defines the line of maximum dip (i.e. perpendicular to the in-situ fracture surface). Therefore, the direction of anisotropy in the samples is in agreement with that observed on the in-situ fracture surface.

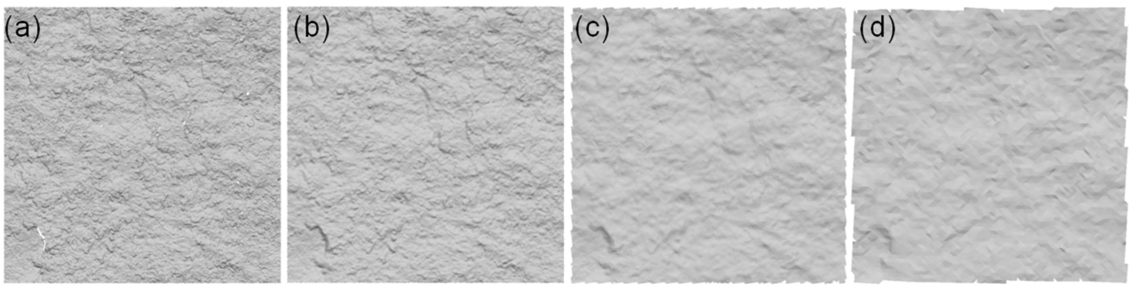

Figure 11. Example of effective smoothing of 3D surface models due to decreasing measurement resolutions. (a), (b), (c), and (d) show the 3D surface models of Sample 1 obtained with an average measurement point spacing of 0.04mm, 0.25mm, 0.50mm, and 1mm, respectively.

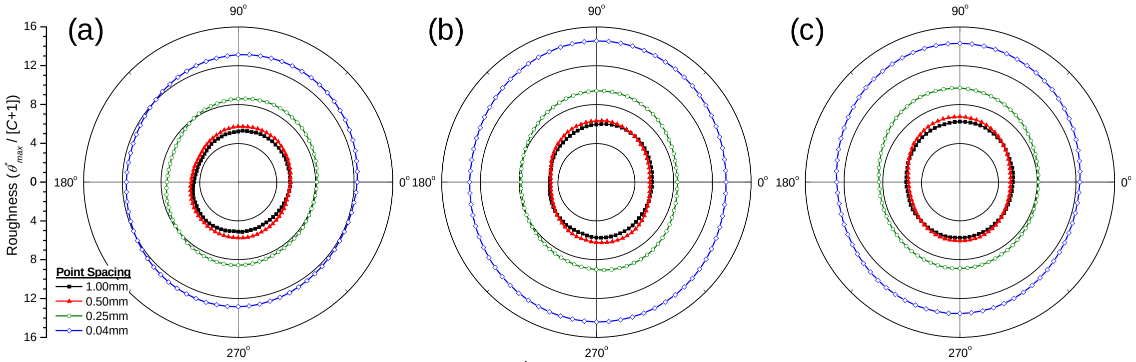

Figure 12. Polar plots of the roughness value, $\theta^{*}_{max}/(C+1)$, for the small-scale fracture samples: (a) Sample 1; (b) Sample 2; and (c) Sample 3. The four series in each plot represent the roughness values corresponding to the average measurement point spacing (resolution) defined in the legend.

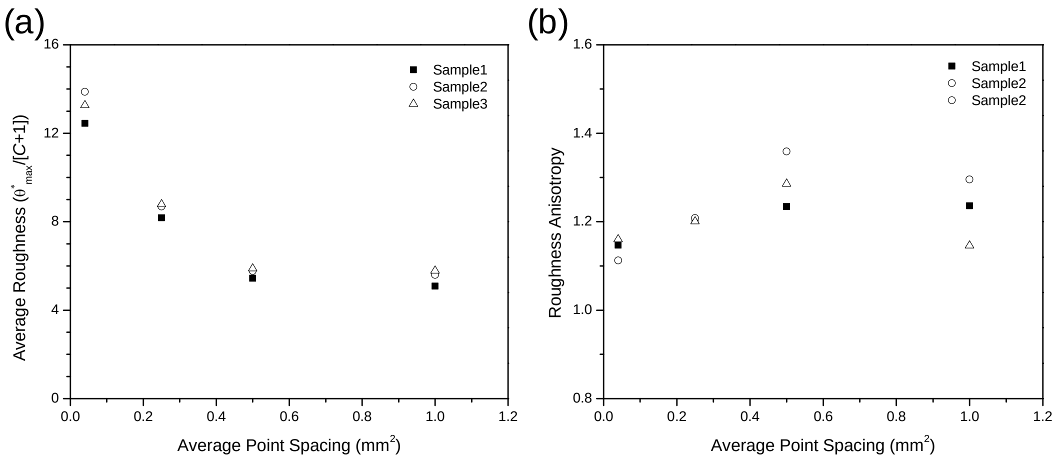

Figure 13. (a) Plot of the average roughness value, $\theta^{*}_{max}/(C+1)$, as a function of the average measurement point spacing. (b) Plot of roughness anisotropy as a function of average point spacing. Although the scatter in anisotropy increases with increased point spacing, it remains close to 1.2 similar to the large-scale results.

4.3 *Discussion*

The main results of this study indicate that discontinuity roughness increases with the size of the sampling window for the same measurement resolution, however, the roughness is very sensitive to the measurement resolution with the value decreasing significantly when the average measurement point spacing is increased. Over the years several authors have investigated the scale dependence on the shear strength of rock discontinuities. Generally, shear strength is thought to show a negative scale effect (i.e. decreasing strength with increasing joint size) partly due to a decrease in asperity strength and partly due to a decrease in roughness with scale. However, as previously mentioned in the introduction of this paper, the scale-dependence of the roughness component is somewhat controversial with some investigations illustrating negative scale effect (Bandis et al. 1981, Fardin et al. 2004, Fardin et al. 2001, Maerz & Franklin 1990, Pratt et al. 1974) and some a positive scale effect (Giani et al. 1992, Hencher et al. 1993, Swan & Zongqi 1985).

Upon reviewing studies which investigated roughness scale dependency via analysis of large-scale surfaces (i.e. profiles or surfaces greater than 1m or 1m^2, respectively), it is apparent that there is potential confusion regarding the influence of sample size and measurement resolution on the calculated roughness. Of all the studies on large-scale fractures (Cravero et al. 2001, Fardin et al. 2004, Fardin et al. 2001, Feng et al. 2003, Maerz & Franklin 1990), all but Fardin et al. (2004) use differing measurement point density (resolution) when digitizing fracture surfaces of varying size. In all these cases, the average measurement point spacing was decreased as larger areas (or lengths) of the fracture surface were considered. Based on the results of the current study, it has been shown that decreasing measurement resolution can significantly reduce the estimated surface roughness. Hence, it is possible that the decrease in roughness with increased fracture size observed in the aforementioned studies maybe caused by the differences in measurement resolution rather than changes of fracture geometry with window size.

Nevertheless, the study of Fardin et al., (2004) also displayed a negative scale effect despite maintaining the same average point spacing (20mm) for all sampling windows. The measurement resolution considered, however, was low compared to the current study (20mm vs. 1mm). Therefore, the smaller scale features of the surface were neglected from the roughness evaluations possibly leading to the alternative relationship between roughness and sample size. As a continuation of the current study, it is planned to analyse one of the series of sampling windows in Figure 8 with the same technique described Fardin et al., (2004, 2001) to determine if the same relationship between roughness and sample window size can be obtained.

Another possible explanation of the positive scale effect observed in this study may be related to the results of Swan & Zongqi (1985). Based on the analysis of 2D profiles, they discovered that for the same profile both positive and negative scale effects could be observed by considering different references line for roughness determination. Considering several sub-samples of a longer profile, it was found that if a unique best-fit reference line for each sample was used to analyse roughness, a positive scale effect could be observed. Meanwhile, if a best-fit line through the entire profile was used as a common reference line for all samples, a negative scale effect was observed. For the current study, a unique best-fit plane was established for each sampling window and a positive scale effect was observed. Thus, it is possible that if the same fracture surface was analysed using the best-fit plane of the entire fracture surface as the reference plane, a negative scale effect may be observed. This analysis is beyond the scope of the current paper but will be considered in the course of future study.

5 CONCLUSIONS

Based on the results of this study the following conclusions can be drawn:

- The ATOS II was successfully employed to digitize a large-scale rock fracture surface in-situ (average point spacing of 1mm) and small-scale samples of said fracture in the laboratory (average point spacing of 0.04mm-1mm) for the purpose of roughness determination.
- The 3D roughness according to the method of Graselli (2006, 2003, 2002) for the large-scale planar fracture surface in granite gneiss displayed a positive scale-effect, which approached a roughly constant value for sufficiently large sampling windows (> 3×10^6 mm^2).
- Via digitization of the small-scale fracture samples in the laboratory, the 3D roughness was shown to be much more sensitive to the measurement resolution adopted to digitize the surface compared to the size of the sampling window. Increasing the average spacing between measurements effectively smooth the surface; resulting in a 79% - 85% percent difference in roughness.
- Anisotropy in roughness was nearly the same for the large-scale and small-scale fracture surfaces and was found to be insensitive to both the sample window size and resolution.

6 ACKNOWLEDGEMENTS

This work has been supported by NSERC in the form of Discovery Grant No. 341275 and RTI Grant No. 345516 held by G. Grasselli and an Alexander Graham Bell Canada Graduate Scholarship held by B.S.A. Tatone. The authors would also like to thank Pulin Mondal for his assistance with the field work required for this study.

REFERENCES

Bandis, S., Lumsden, A. C., & Barton, N. R., 1981. Experimental studies of scale effects on the shear behavior of rock joints. *International Journal of Rock Mechanics and Mining Sciences*, (18)1: 1-21.

Barton, N., 1973. Review of a new shear-strength criterion for rock joints. *Engineering Geology*, (7)4: 287-332.

Barton, N., & Choubey, V., 1977. The shear strength of rock joints in theory and practice. *Rock Mechanics and Rock Engineering*, (10)1: 1-54.

Cravero, M., Iabichino, G., & Ferrero, A. M. 2001. Evaluation of joint roughness and dilatancy of schistosity joints. In P. Sarkka, &P. Eloranta (eds.), *Rock mechanics - a challenge for society; proceedings of Eurock 2001, Espoo, Finland, 4-7 June 2001*: 217-222. Rotterdam: A.A. Balkema.

Fardin, N., Feng, Q., & Stephansson, O., 2004. Application of a new in situ 3d laser scanner to study the scale effect on the rock joint surface roughness. *International Journal of Rock Mechanics and Mining Sciences*, (41)2: 329-335.

Fardin, N., Stephansson, O., & Jing, L., 2001. The scale dependence of rock joint surface roughness. *International Journal of Rock Mechanics and Mining Sciences*, (38)5: 659-669.

Feng, Q., Fardin, N., Jing, L., & Stephansson, O., 2003. A new method for in-situ non-contact roughness measurement of large rock fracture surfaces. *Rock Mechanics and Rock Engineering*, (36)1: 3-25.

Giani, G. P., Ferrero, A. M., Passarello, G., & Reinaudo, L. 1992. Scale effect evaluation on natural discontinuity shear strength. In L. R. Myers, C. F. Tsang, N. G. W. Cook, &R. E. Goodman (eds.), *Proceedings of the conference on fractured and jointed rock masses, Lake Tahoe, CA, 3-5 June 1993*: 447-452. Rotterdam: A.A. Balkema.

GOM, 2008. *Atos user manual v. 6.1*. Braunschweig, Germany: GOM mbH

Grasselli, G., 2006. Manuel rocha medal recipient - shear strength of rock joints based on quantified surface description. *Rock Mechanics and Rock Engineering*, (39)4: 295-314.

Grasselli, G., & Egger, P., 2003. Constitutive law for the shear strength of rock joints based on three-dimensional surface parameters. *International Journal of Rock Mechanics and Mining Sciences*, (40)1: 25-40.

Grasselli, G., Wirth, J., & Egger, P., 2002. Quantitative three-dimensional description of a rough surface and parameter evolution with shearing. *International Journal of Rock Mechanics and Mining Sciences*, (39)6: 789-800.

Grasselli, G., Wirth, J., & Zimmerman, R. W. 2002b. Functional parameters for quantifying the surface anisotropy of rock discontinuities. In W. Wittke (ed.), *ISRM International symp. on rock engineering for mountainous regions; proceedings of Eurock 2002, Funchal (Madeira Island), Portugal, November 25-28, 2002*: 722-733.

Haneberg, W. 2007. Directional roughness profiles from three-dimensional photogrammetric or laser scanner point clouds. In E. Eberhardt, D. Stead, &T. Morrison (eds.), *Rock Mechanics: Meeting Society's Challenges and Demands; proceedings of the 1st Canada-US rock mechanics symposium, Vancouver, Canada, 27-31 May 2007*: 101-106. London: Taylor and Francis.

Hencher, S. R., Toy, J. P., & Lumsden, A. C. 1993. Scale-dependent shear-strength of rock joints. In *Scale Effects in Rock Masses 93; Proceedings of the 2nd international workshop on scale effects in rock masses, Lisbon, Portugal, 25 June 1993*: 233-240. Rotterdam: A.A. Balkema.

Hong, E. S., Lee, I. M., & Lee, J. S., 2006. Measurement of rock joint roughness by 3d scanner. *Geotechnical Testing Journal*, (29)6: 482-489.

ISRM, 1978. International society for rock mechanics commission on standardization of laboratory and field tests: Suggested methods for the quantitative description of discontinuities in rock masses. *International Journal of Rock Mechanics and Mining Sciences & Geomechanics Abstracts*, (15)6: 319-368.

Ladanyi, B., & Archambault, G. 1970. Simulation of the shear behaviour of a jointed rock mass. In *Proceedings of the 11th Symposium on Rock Mechanics: Theory and Practice, Berkeley, CA, 1969*: 105-125. New York: American Institute of Mining Engineers.

Maerz, N. H., & Franklin, J. A. 1990. Roughness scale effects and fractal dimension. In A. Pinto Da Cunha (ed.), *Scale effects in rock masses; proceedings of the first international workshop on scale effects in rock masses, Loen, Norway, 7-8 June 1990*: 121-125. Rotterdam: A.A. Balkema.

Nasseri, M. H. B., Tatone, B. S. A., Grasselli, G., & Young, R. P., 2009. Fracture toughness and fracture roughness interrelationship in thermally treated westerly granite. *Pure and Applied Geophysics* (in press).

Patton, F. D. 1966. Multiple modes of shear failure in rock. In *Proceeding of the1st Congress of International Society of Rock Mechanics, Lisbon, Portugal*: 509-513.

Pratt, H. R., Black, A. D., & Brace, W. F. 1974. Friction and deformation of jointed quartz diorite. In *Advances in rock mechanics; reports of current research; Proceedings of the 3rd Congress of ISRM, Denver, CO, September 1-7 1974*: 306-310. Washington, D.C.: National Academy of Sciences.

Rasouli, V., & Harrison, J. P., 2004. A comparison of linear profiling and an in-plane method for the analysis of rock surface geometry. *International Journal of Rock Mechanics and Mining Sciences*, (41)3: 377-378.

Riss, J., & Gentier, S. 1990. Angularity of a natural rock fracture. In H. P. Rossmanith (ed.), *Mechanics of Jointed and Faulted Rock, Vienna, 18-20 April 1990*: 399-406. Rotterdam: A.A. Balkema.

Swan, G., & Zongqi, S., 1985. Prediction of shear behavior of joints using profiles. *Rock Mechanics and Rock Engineering*, (18)3: 183-212.